Potentially biogenic carbon preserved in a 4.1 billion-year-old zircon

Elizabeth A. Bell[a,1], Patrick Boehnke[a], T. Mark Harrison[a,1], and Wendy L. Mao[b]

[a]Department of Earth, Planetary, and Space Sciences, University of California, Los Angeles, CA 90095; and [b]School of Earth, Energy, and Environmental Sciences, Stanford University, Stanford, CA 94305

Contributed by T. Mark Harrison, September 4, 2015 (sent for review July 31, 2015)

Evidence of life on Earth is manifestly preserved in the rock record. However, the microfossil record only extends to ∼3.5 billion years (Ga), the chemofossil record arguably to ∼3.8 Ga, and the rock record to 4.0 Ga. Detrital zircons from Jack Hills, Western Australia range in age up to nearly 4.4 Ga. From a population of over 10,000 Jack Hills zircons, we identified one >3.8-Ga zircon that contains primary graphite inclusions. Here, we report carbon isotopic measurements on these inclusions in a concordant, 4.10 ± 0.01-Ga zircon. We interpret these inclusions as primary due to their enclosure in a crack-free host as shown by transmission X-ray microscopy and their crystal habit. Their $\delta^{13}C_{PDB}$ of −24 ± 5‰ is consistent with a biogenic origin and may be evidence that a terrestrial biosphere had emerged by 4.1 Ga, or ∼300 My earlier than has been previously proposed.

Hadean | carbon isotopes | early Earth | zircon | origin of life

Life on Earth is an ancient phenomenon, with the earliest identified microfossils at nearly 3.5 billion years before present (Ga) (1) and the earliest potential chemofossils at 3.83 Ga (2, 3). Investigation of older materials is limited by the increasingly sparse and metamorphosed rock record, with the oldest rock age at 4.0 Ga (ref. 4; cf. ref. 5). Given the temporal limits of the rock record, it has been difficult to assess terrestrial habitability or document a biosphere before ∼3.8 Ga. Despite the lack of a rock record before 4.0 Ga, detrital zircons as old as 4.38 Ga have been documented (6). About 5% of the zircons from a ∼3-Ga metaconglomerate at Jack Hills, Western Australia yield ages greater than 3.8 Ga (6). Their geochemistry and mineral inclusions have been interpreted to indicate their derivation largely from hydrous, sediment-derived granitic magmas (7–12). The relatively clement conditions implied suggest a potentially habitable planet and leave open the possibility of a Hadean (>4-Ga) biosphere.

The stable isotope ratio $^{13}C/^{12}C$ (herein defined relative to the Pee Dee Belemnite standard, i.e., $\delta^{13}C_{PDB}$) provides a potential biosignature due to the isotopic fractionation that occurs during carbon fixation. As a consequence, biogenically derived kerogens yield an average of −25 ± 10‰ across the sedimentary rock record from 3.4 Ga to the present (13), whereas carbonates and mantle values are consistently offset with averages of 0‰ (13) and −5‰ (14), respectively. Thus, the discovery of isotopically light graphite in Eoarchean metasediments from southern West Greenland (2, 15) was proposed as evidence of a 3.7- to 3.8-Ga biosphere.

The >3.8-Ga Jack Hills zircons contain abundant mineral inclusions, mostly of a granitic character (11). Abundant and intimately associated diamond and graphite (4% of each in the zircons investigated) were reported in previous studies (16, 17) but subsequently shown to be diamond polishing debris and epoxy that had lodged in cracks during sample preparation (18). This left the true occurrence and abundance of carbonaceous materials in the Jack Hills zircons uncertain. We imaged a large number of >3.8-Ga Jack Hills zircons in search of carbonaceous inclusions and made carbon isotopic measurements of primary graphite found in one grain. To our knowledge, we report here the first unambiguous carbon isotopic measurements of terrestrial Hadean material.

Results

From an initial population of over 10,000 Jack Hills zircons (6), we examined 656 grains with ages over 3.8 Ga for the presence of graphitic inclusions. The zircons were mounted in epoxy and polished to expose their interiors. The search protocol included an initial screening for opaque inclusions using transmitted light microscopy. Seventy-nine candidates thus identified were then targeted for Raman spectroscopy from which we documented two zircons containing partially disordered graphite (Fig. 1, *Inset*) beneath their polished surfaces (RSES 81-10.14 in a cracked region; RSES 61-18.8 in a crack-free region). We did not consider RSES 81-10.14 further due to the potential for contamination via ingress on cracks.

A concordant U-Pb age of 4.10 ± 0.01 Ga was obtained on a polished internal surface of zircon RSES 61-18.8 (6). Its low U content (∼100 ppm; *Supporting Information*) minimizes the potential for radiation damage and is a contributing cause for its 99% U-Pb concordancy (6). A roughly 30 × 60 × 20-μm sliver containing two carbonaceous phases was milled using a Ga^+ focused ion beam (FIB) and attached to a tungsten needle via a platinum weld for synchrotron transmission X-ray microscopy (19) at beam line 6-2c of the Stanford Synchrotron Radiation Lightsource (SSRL). The 40-nm spatial resolution of this imaging method revealed no through-going cracks or defects associated with these inclusions that exhibit the graphite crystal habit (Fig. 1; also *Supporting Information*). Due to their isolation within a crack-free region of an isotopically undisturbed zircon, conditions shown to preserve primary inclusion assemblages (20), we interpret these graphitic inclusions to have been incorporated during crystallization of this igneous zircon.

Significance

Evidence for carbon cycling or biologic activity can be derived from carbon isotopes, because a high $^{12}C/^{13}C$ ratio is characteristic of biogenic carbon due to the large isotopic fractionation associated with enzymatic carbon fixation. The earliest materials measured for carbon isotopes at 3.8 Ga are isotopically light, and thus potentially biogenic. Because Earth's known rock record extends only to ∼4 Ga, earlier periods of history are accessible only through mineral grains deposited in later sediments. We report $^{12}C/^{13}C$ of graphite preserved in 4.1-Ga zircon. Its complete encasement in crack-free, undisturbed zircon demonstrates that it is not contamination from more recent geologic processes. Its ^{12}C-rich isotopic signature may be evidence for the origin of life on Earth by 4.1 Ga.

Author contributions: E.A.B., P.B., and T.M.H. designed research; E.A.B., P.B., and T.M.H. performed research; W.L.M. contributed new reagents/analytic tools; E.A.B., P.B., and T.M.H. analyzed data; and E.A.B., P.B., and T.M.H. wrote the paper.

The authors declare no conflict of interest.

Freely available online through the PNAS open access option.

[1]To whom correspondence may be addressed. Email: ebell21@ucla.edu or tmark.harrison@gmail.com.

This article contains supporting information online at www.pnas.org/lookup/suppl/doi:10.1073/pnas.1517557112/-/DCSupplemental.

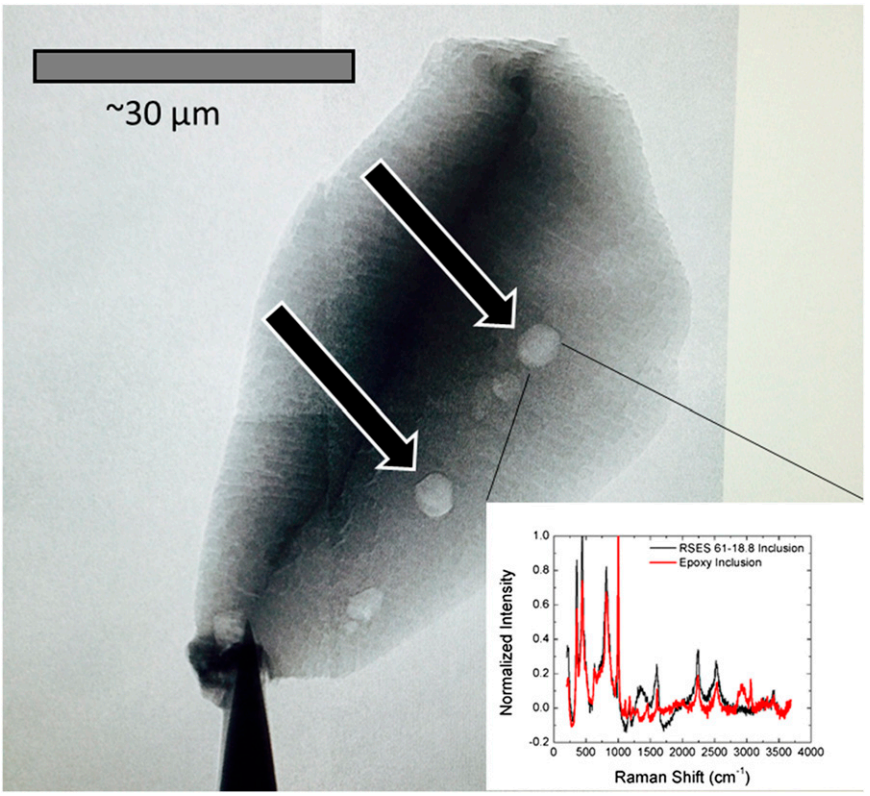

Fig. 1. Transmission X-ray image of RSES 61-18.8 with graphite indicated. (*Inset*) Raman spectra for the top inclusion and for an epoxy "inclusion" from another investigated zircon. The broadened "D-band" at ~1,400 cm^{-1} indicates disordered graphite (39); C–H stretch bands at ~2,800–3,100 cm^{-1} (39) are observed in epoxy but not graphite.

The zircon sliver was remounted in indium, coated with gold, and analyzed for $\delta^{13}C$ on a CAMECA *ims*1270 secondary ion mass spectrometer (SIMS) using a 5-nA Cs^+ primary beam (21) with static multicollection following a 2-min cleaning via rastering of the primary beam. Note that the two inclusions had not previously been exposed to epoxy or any other source of laboratory carbon contamination and were revealed only by drilling with the primary Cs^+ ion beam. During analysis of the smaller inclusion, we found that count rates increased to a maximum value as the inclusion was breached followed by a tailing to background (*Supporting Information*). This precludes the possibility that our data were affected by surface contamination.

SIMS measurement of C isotopes in carbonaceous materials is known to be little affected by instrumental mass fractionation. For example, a previous study found less than 2‰ variation in an intercomparison of hydrocarbon standards that varied in H/C by a factor of 7 (21). Thus, we used epoxy, with $\delta^{13}C$ of −26.8‰ (21), as a standard material for instrumental mass fractionation corrections and *Escherichia coli* with $\delta^{13}C$ of −24‰ (21) as a secondary standard. The two inclusions yielded similar results in both carbon abundance and $\delta^{13}C$. Maximum signals of ~10^5 counts per second (cps) of $^{12}C_2{}^+$ for the inclusions was at least an order of magnitude higher than for the C background in the indium mounting material (~10^4 cps) and much higher than a clean area in the zircon (~10^3 cps). The $\delta^{13}C$ values of the two inclusions are indistinguishable within error, and thus we combined the results to obtain an average of −24 ± 5‰. This is notably light with respect to terrestrial inorganic carbon and most meteoritic carbon, but consistent with terrestrial biogenic carbon (Fig. 2). Following carbon isotopic analysis, we measured rare earth element (REE) and Ti abundances using the *ims*1270 with a 15-nA O^- primary beam. Two spots yielding measurable Ti correspond to an average apparent crystallization temperature of ~660 °C, similar to the average Hadean Jack Hills value (9), with REE consistent with crystallization under reduced conditions (using the method of ref. 22) and a continental trace element signature (following the discriminant diagrams of ref. 23).

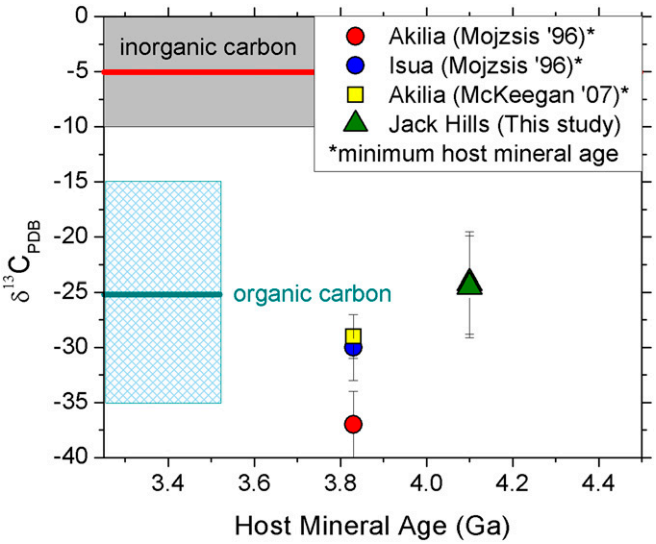

Fig. 2. $\delta^{13}C$ for Eoarchean–Hadean carbon samples measured via SIMS vs. host mineral age compared with inorganic and organic carbon (organic carbon values from ref. 13; inorganic from ref. 14).

Discussion

Given the isolation of these inclusions provided by their entrapment in a crack-free and isotopically undisturbed zircon crystal, as well as the vanishingly slow self-diffusion of carbon in graphite under crustal conditions (24), we interpret them to be petrologically primary and isotopically closed systems. Because these inclusions are at least as old as their 4.10-Ga host, the observation of isotopically light carbon raises the possibility that biologic processes were operating during the Hadean. To be sure, not all light carbon isotopic signals are biogenic.

Abiotic processes that could produce light $\delta^{13}C$ during the Hadean include Fischer–Tropsch mechanisms (25) and carbon isotopic fractionation by diffusion (26), incorporation of meteoritic (ranging from +68‰ to −60‰ $\delta^{13}C$) materials, mid-ocean ridge basalt degassing (27), and high-temperature disproportionation of siderite (28). However, in the absence of experimental evidence for particulate carbon formation via a Fischer–Tropsch process (ref. 25; cf. ref. 27) or diffusive or mineral disproportionation mechanisms that could selectively lead to light carbon condensates that were ultimately incorporated in a low-temperature (i.e., ∼650 °C) granitoid zircon, a biogenic origin seems at least as plausible. The quantity of extraterrestrial carbon necessary to dominate the carbon budget of a felsic magma protolith would be significant and profoundly influence the chemistry of that magma away from its granitoid character unless separated from the host meteorite. A possible mechanism to effect this on ancient Earth might be through sedimentary processing and concentration of meteoritic carbon in pelagic sediments. Even if meteoritic carbon could be concentrated in this fashion, our observed isotopic signal is uncharacteristic of the most likely candidates, carbonaceous chondrites, which contain on average 3.5 wt% C (29). Although $\delta^{13}C$ of various components ranges between +68‰ and −34‰ (30), only 10% of bulk carbon measurements have $\delta^{13}C$ less than −20‰ (31), and thus this class of meteorites would be a fortuitous, although possible, source for both inclusions. Our view that isotopically light C in ancient terrestrial materials may be of biogenic origin is consistent with interpretations of light $\delta^{13}C$ in mantle diamonds (e.g., ref. 32). Although diamonds as low as approximately −10‰ are able to be accounted for by isotopic fractionation of abiogenic precursors, more negative values down to −23‰ do not appear to be explicable by such processes and strongly suggest an origin from subducted organic matter (33). Although we cannot rule out an abiogenic source, the eventual acquisition of a large database of Hadean carbon isotope measurements will permit the plausibility of hypothetical abiogenic origins to be more closely scrutinized.

By contrast, biogenic organic matter is incorporated into the vast majority of preserved clastic sediments, can reach 10% by weight in Phanerozoic sediments (34), and has averaged $\delta^{13}C$ approximately −25‰ over the past 3.5 Ga (13). Given this historical trend and the several lines of evidence indicative of sediment involvement in the Jack Hills zircon magmas (8, 10–12), the simplest interpretation of our data are that the carbonaceous inclusions represent graphitized organic carbon present during melting of a pelitic protolith at 4.10 Ga. This interpretation is entirely consistent with the observed low crystallization temperature, continental affinity, and reduced environment (35) of zircon formation.

The isolated, primary nature of the graphite in sample RSES 61-18.8, along with the lack of diamond features in its Raman spectrum, differs from the abundant graphite previously reported (16, 17) in Jack Hills zircons, which was found often intersecting cracks in the host zircon, and all of which were reported to contain diamond (17). As noted, the diamonds were later found to be contamination (18). The rare occurrence of primary graphite in this study (in <0.2% of >3.8-Ga zircons) also contrasts with these earlier results (graphite in 4% of zircons of all ages), further suggesting that much or all of the earlier-purported graphite identified was contamination.

There are considerable limitations of basing any inference regarding early Earth on a single zircon containing primary carbonaceous inclusions. Instead, we see this contribution as demonstrating the feasibility of perhaps the only approach that could lead to establishing a Hadean carbon isotope record. In this regard, we emphasize that because >3.8-Ga grains make up only ∼5% of the Jack Hills zircon population (6), RSES 61-18.8 represents an abundance of carbon-bearing Jack Hills zircons of only about 1-in-10,000.

Conclusions

This study extends the terrestrial carbon isotope record ∼300 My beyond the previously oldest-measured samples from southwest Greenland. Our interpretation that the light C isotope signature in primary graphitic inclusions could reflect biologic processes is consistent with an estimate from molecular divergence in prokaryote phylogenetic relationships that a terrestrial biosphere had emerged by 4.1 Ga (36). Confirming such a connection would represent a potentially transformational scientific advance. However, given the low occurrence of carbon-bearing Hadean zircons, establishing a Hadean carbon cycle and its possible bearing on the origin of life will require enormous and sustained efforts.

Methods

Zircons were mounted in epoxy and polished to expose their interiors, typically involving loss of approximately one-third of the zircon during polishing. Polishing was accomplished with 1,200-grit silicon carbide paper and 1-μm diamond paste. The search protocol included an initial screening for opaque inclusions using transmitted light microscopy and a 40× objective lens.

Raman Spectroscopy. Confocal Raman spectroscopy was carried out on zircons mounted in epoxy in several laboratories, using a green laser and 20× or 40× objective lenses. Opaque inclusions noted by transmitted light microscopy were analyzed for carbonaceous material. This screening procedure includes some inherent bias toward zircons clear enough for effective transmitted light microscopy, although this appears to include most of the Hadean Jack Hills population imaged in this study. We also note that our screening protocol does not completely preclude some of the other opaque inclusions from containing some carbonaceous material—the Raman signal could be masked by high noise.

FIB Milling. Sample RSES 61-18.8 was coated in gold and a ∼60 × 30 × 20 triangular prismatic region containing the identified carbonaceous inclusion was milled from the larger zircon sample using a Nova 600 SEM/FIB system at the University of California, Los Angeles (UCLA) Nanoelectronics Research Facility. The section of zircon was attached to a tungsten needle using a platinum weld.

X-Ray Microscopy. The FIBed section of RSES 61-18.8 was imaged by transmission X-ray microscopy at beam line 6-2c of the SSRL (19), at a spatial resolution of 40 nm. An energy of 7,160 eV was used for imaging. One X-ray image is seen in Fig. 1, while movies constructed from the X-ray slices are presented in *Supporting Information*.

Carbon Isotopic Measurements. We used the method of ref. 3, modified for static multicollection. We also included a 2-min precleaning of analysis surfaces with a 20 × 20-μm raster of the primary beam. We used a Cs^+ primary beam of 5 nA for measurements on *E. coli* and zircon samples and of 2 pA for measurements on the epoxy. We used epoxy as our primary standard (−26.8‰ PDB; ref. 21) for all instrumental mass fractionation corrections and *E. coli* as a secondary standard (−24.1; our analyses averaged −19 ± 4‰).

Error bars on our graphite inclusions incorporate the internal error bars for the analyses, the reproducibility of the epoxy, and quadratic addition of a 4‰ uncertainty due to potential matrix effects between epoxy and graphite (21). The latter is included even though negligible matrix effects were noticed in an earlier study, where less than 2‰ variation was observed in an intercomparison of hydrocarbon standards that varied in H/C by a factor of 7 (21). Considering these error bars, normalization to either the primary epoxy or secondary *E. coli* standard produces statistically indistinguishable $\delta^{13}C_{PDB}$ values for our inclusions.

Trace Element Measurement. These analyses were carried out using a CAMECA *ims*1270 ion microprobe at UCLA, with primary O^- beam intensity of ~15 nA and a spot size of 60 μm. Secondary ions were detected at high energy offset (–100 eV) to suppress molecular interferences. Further peak stripping for background and isobaric interference corrections was accomplished off-line. Standardization was to the National Institute of Standards and Technology 610 standard glass, with the 91500 zircon (37) used as a secondary standard. Additional correction of [Ti] used a value for 91500 of 5.2 ± 0.3 ppm (38).

ACKNOWLEDGMENTS. Raman spectroscopy by Anatoliy Kudryavtsev, Anke Watenpuhl, Olivier Beyssac, and Daniel Wilkinson, using confocal Raman systems in the laboratories of William Schopf, Andrew Steele, Olivier Beyssac, and Bruce Dunn, made possible our search for carbonaceous inclusions. FIB milling by Noah Bodzin, X-ray imaging by Wendy Mao and Crystal Shi [who are supported by National Science Foundation (NSF)–Division of Earth Sciences (EAR) Grant 1055454], and sample mounting by Christopher Snead were also essential. We thank Elizabeth Boehnke for X-ray image reconstruction and for Movie S2. We thank the three reviewers, whose comments greatly improved our manuscript. This project was funded by a Simons Collaboration on the Origin of Life Postdoctoral Fellowship (to E.A.B.) and NSF-EAR Grant 0948724 (to T.M.H.). The UCLA ion microprobe facility is partially supported by a grant from the Instrumentation and Facilities Program of EAR, NSF. Data reported in this manuscript are presented in full in *Supporting Information*. Portions of this research were carried out at the SSRL, a Directorate of SLAC National Accelerator Laboratory and an Office of Science User Facility operated for the US Department of Energy, Office of Science by Stanford University.

1. Awramik SM (1992) The oldest records of photosynthesis. *Photosynth Res* 33:75–89.
2. Mojzsis SJ, et al. (1996) Evidence for life on Earth before 3,800 million years ago. *Nature* 384(6604):55–59.
3. McKeegan KD, Kudryavtsev AB, Schopf JW (2007) Raman and ion microscopic imagery of graphitic inclusions in apatite from older than 3830 Ma Akilia supracrustal rocks, West Greenland. *Geology* 35(7):591–594.
4. Bowring SA, Williams IS (1999) Priscoan (4.00–4.03 Ga) orthogneisses from northwestern Canada. *Contrib Mineral Petrol* 134(1):3–16.
5. O'Neil J, Carlson RW, Francis D, Stevenson RK (2008) Neodymium-142 evidence for Hadean mafic crust. *Science* 321(5897):1828–1831.
6. Holden P, et al. (2009) Mass-spectrometric mining of Hadean zircons by automated SHRIMP multi-collector and single-collector U/Pb zircon age dating: The first 100,000 grains. *Int J Mass Spectrom* 286(2):53–63.
7. Maas R, Kinny PD, Williams IS, Froude DO, Compston W (1992) The Earth's oldest known crust: A geochronological and geochemical study of 3900–4200 Ma old detrital zircons from Mt. Narryer and Jack Hills, Western Australia. *Geochim Cosmochim Acta* 56(3):1281–1300.
8. Mojzsis SJ, Harrison TM, Pidgeon RT (2001) Oxygen-isotope evidence from ancient zircons for liquid water at the Earth's surface 4,300 Myr ago. *Nature* 409(6817):178–181.
9. Watson EB, Harrison TM (2005) Zircon thermometer reveals minimum melting conditions on earliest Earth. *Science* 308(5723):841–844.
10. Harrison TM (2009) The Hadean crust: Evidence from >4 Ga zircons. *Annu Rev Earth Planet Sci* 37:479–505.
11. Hopkins M, Harrison TM, Manning CE (2010) Constraints on Hadean geodynamics from mineral inclusions in >4 Ga zircons. *Earth Planet Sci Lett* 298(3):367–376.
12. Peck WH, Valley JW, Wilde SA, Graham CM (2001) Oxygen isotope ratios and rare earth elements in 3.3–4.4 Ga zircons: Ion microprobe evidence for high $\delta^{18}O$ continental crust and oceans in the Early Archean. *Geochim Cosmochim Acta* 65(22):4215–4299.
13. Schopf JW, Kudryavtsev AB (2014) Biogenicity of Earth's earliest fossils. *Evolution of Archean Crust and Early Life*, Modern Approaches in Solid Earth Sciences, eds Dilek Y, Furnes H (Springer, Dordrecht, The Netherlands), Vol 7, pp 333–349.
14. Hoefs J (1973) *Stable Isotope Geochemistry* (Springer, Berlin).
15. Rosing MT (1999) ^{13}C-depleted carbon microparticles in >3700-Ma sea-floor sedimentary rocks from west greenland. *Science* 283(5402):674–676.
16. Menneken M, Nemchin AA, Geisler T, Pidgeon RT, Wilde SA (2007) Hadean diamonds in zircon from Jack Hills, Western Australia. *Nature* 448(7156):917–920.
17. Nemchin AA, et al. (2008) A light carbon reservoir recorded in zircon-hosted diamond from the Jack Hills. *Nature* 454(7200):92–95.
18. Dobrzhinetskaya L, Wirth R, Green H (2014) Diamonds in Earth's oldest zircons from Jack Hills conglomerate, Australia, are contamination. *Earth Planet Sci Lett* 387:212–218.
19. Andrews JC, et al. (2010) Nanoscale X-ray microscopic imaging of mammalian mineralized tissue. *Microsc Microanal* 16(3):327–336.
20. Bell EA, Boehnke P, Hopkins-Wielicki MD, Harrison TM (2015) Distinguishing primary and secondary inclusion assemblages in Jack Hills zircons. *Lithos* 234:15–26.
21. House CH, et al. (2000) Carbon isotopic composition of individual Precambrian microfossils. *Geology* 28(8):707–710.
22. Trail D, Watson EB, Tailby ND (2011) The oxidation state of Hadean magmas and implications for early Earth's atmosphere. *Nature* 480(7375):79–82.
23. Grimes CB, et al. (2007) Trace element chemistry of zircons from oceanic crust: A method for distinguishing detrital zircon provenance. *Geology* 35(7):643–646.
24. Thrower PA, Mayer RM (1978) Point defects and self-diffusion in graphite. *Phys Status Solidi* 47(1):11–37.
25. McCollom TM (2013) Laboratory simulations of abiotic hydrocarbon formation in Earth's deep subsurface. *Rev Mineral Geochem* 75:467–494.
26. Mueller T, et al. (2014) Diffusive fractionation of carbon isotopes in γ-Fe: Experiment, models and implications for early solar system processes. *Geochim Cosmochim Acta* 127:57–66.
27. Shilobreeva S, et al. (2011) Insights into C and H storage in the altered oceanic crust: Results from ODP/IODP Hole 1256D. *Geochim Cosmochim Acta* 75(9):2237–2255.
28. Van Zuilen MA, Lepland A, Arrhenius G (2002) Reassessing the evidence for the earliest traces of life. *Nature* 418(6898):627–630.
29. McDonough WF, Sun S-s (1995) The composition of the Earth. *Chem Geol* 120(3):123–153.
30. Marty B, Alexander CMD, Raymond SN (2013) Primordial origins of Earth's carbon. *Rev Mineral Geochem* 75:149–181.
31. Kerridge JF (1985) Carbon, hydrogen and nitrogen in carbonaceous chondrites: Abundances and isotopic compositions in bulk samples. *Geochim Cosmochim Acta* 49(8):1707–1714.
32. Pearson DG, Canil D, Shirey SB (2003) Mantle samples included in volcanic rocks: Xenoliths and diamonds. *Treatise on Geochemistry* (Elsevier, Amsterdam), Vol 2, pp 171–275.
33. Stachel T, Harris JW, Muehlenbachs K (2009) Sources of carbon in inclusion bearing diamonds. *Lithos* 112:625–637.
34. Hunt MJ (1979) *Petroleum Geochemistry and Geology* (W. H. Freeman and Company, New York).
35. French BM (1966) Some geological implications of equilibrium between graphite and a C-H-O gas phase at high temperatures and pressures. *Rev Geophys* 4(2):223–253.
36. Battistuzzi FU, Feijao A, Hedges SB (2004) A genomic timescale of prokaryote evolution: Insights into the origin of methanogenesis, phototrophy, and the colonization of land. *BMC Evol Biol* 4(1):44.
37. Wiedenbeck M, et al. (2004) Further characterization of the 91500 zircon crystal. *Geostds Geoan Res* 28(1):9–39.
38. Fu B, et al. (2008) Ti-in-zircon thermometry: Applications and limitations. *Contrib Mineral Petrol* 156(2):197–215.
39. Fries M, Steele A (2010) Raman spectroscopy and confocal Raman imaging in mineralogy and petrography. *Confocal Raman Microscopy*, Springer Series in Optical Sciences, eds Dieing T, Hollricher O, Toporski J (Springer, New York), Vol 158, pp 111–135.

Supporting Information

Bell et al. 10.1073/pnas.1517557112

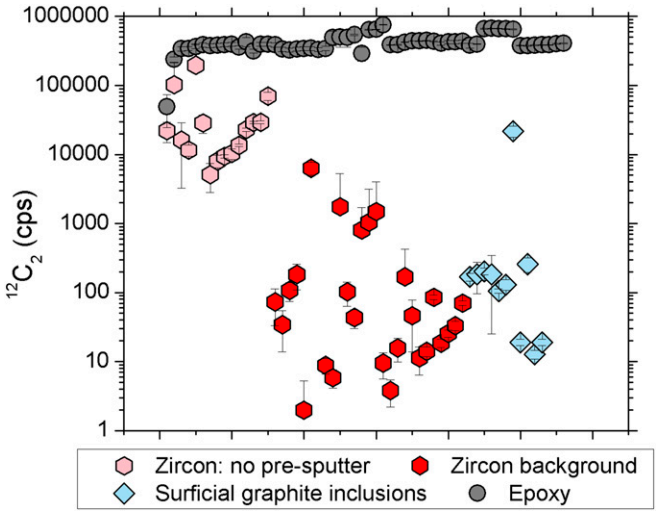

Fig. S1. Carbon signals for background measurements made on other zircons (some Jack Hills zircons, some more recent granite zircons). Carbon signal on *y* axis, analysis number within each group of analyses on *x* axis. "Surficial graphite inclusions" are regions on the polished surfaces of Hadean Jack Hills zircons identified as disordered graphite by Raman analysis. There is little evidence in the ion microprobe data for significant graphite in these regions, suggesting they were surficial contamination from previous sample preparation procedures. Data are presented in Table S1.

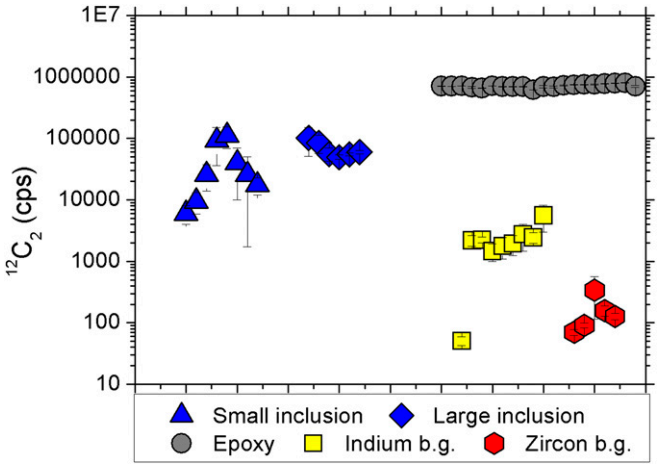

Fig. S2. Carbon signals for analyses on the mount RSES 61-18.8. Carbon signal on *y* axis, analysis number within each group of analyses on *x* axis. "B.g.," background, taken after presputtering to clean the analysis surface of potentially contaminating carbon. Data are presented in Table S2.

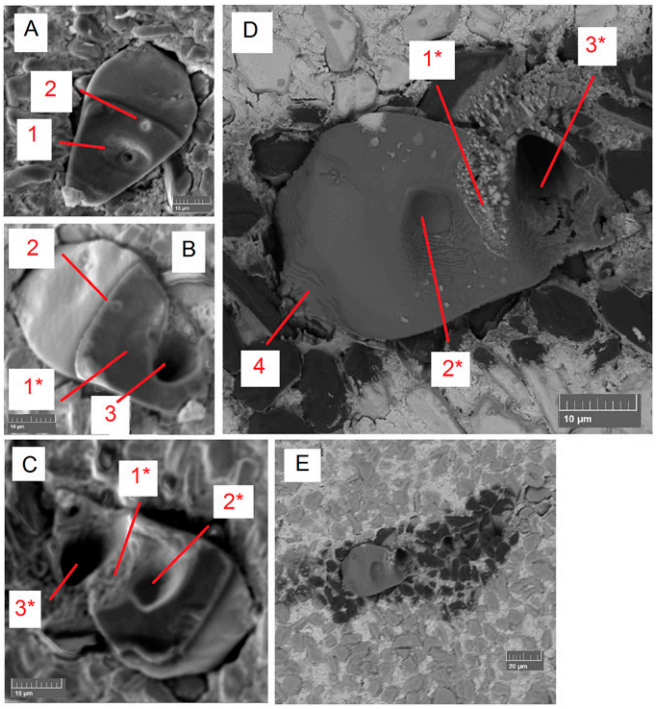

Fig. S3. Electron images taken in between analyses on RSES 61-18.8. (*A*) Secondary electron (SE) image after first measurements that did not find inclusions ("zircon," "zircon_try2" in Tables S2 and S3). Initial analysis pit is indicated by "1," and large inclusion is indicated by "2." Note the larger rastered area that was precleaned before isotopic analysis (dark area). The hexagonal spot in analysis pit 1 is one of the smaller, noncarbonaceous inclusions evident in Movies S1 and S2. (*B*) SE image taken after measurement of small inclusion in "3" ("zircon_try3"). Remnant of "1" pit is also seen. (*C*) SE image of zircon after measurement of large inclusion ("zircon_try8"). Note the larger precleaned area from a second rastering before measurement of the large inclusion, which cleaned the surface surrounding "2." "3*" is the carbon background measurement in a slightly different location than "3," but partially erasing the earlier pit. (*D*) Backscattered electron image (BSE) after all carbon isotope and some trace element measurements. "2*" indicates the pit used for analyzing the large inclusion. Trace element analysis spot 2b is shown by "4." (*E*) BSE image showing a wider view of the zircon mounted in In after carbon isotopic and trace element analyses. Analysis spots are unlabeled.

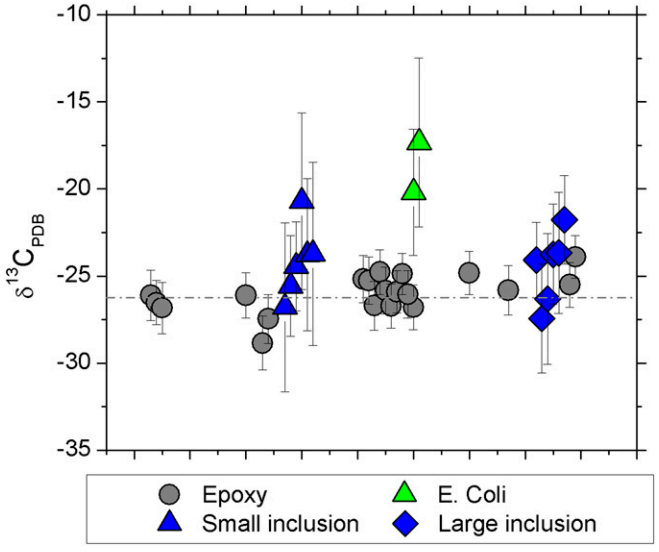

Fig. S4. Corrected $\delta^{13}C$ of epoxy and inclusions on mount RSES 61-18.8. 1σ error bars are shown. Secondary standard *E. coli* is also shown. All analyses are corrected to the epoxy standard (−26.8‰ PDB; ref. 21). The dashed line is at −26.8; corrected epoxy measurements mostly plot within error of the correct value. *E. coli* should be at −24.1‰ (21). *E. coli* measurements average −19 ± 4‰.

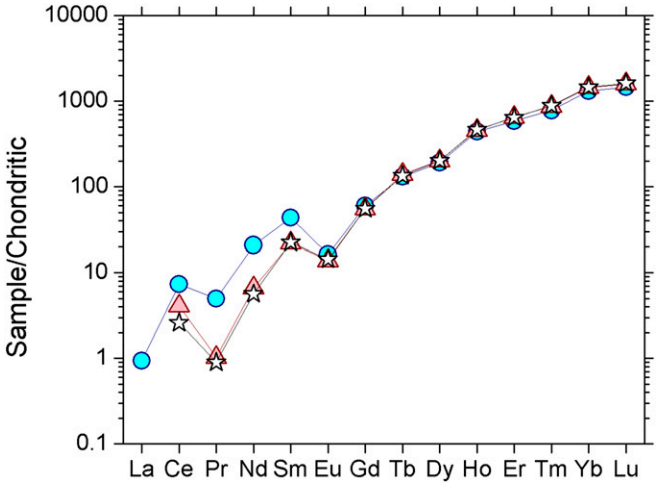

Fig. S5. Rare earth elements (REEs) in sample RSES 61-18.8, normalized to chondritic abundances. The cerium anomaly is calculated as $Ce_N/(La_N \times Pr_N)^{1/2}$ ($_N$ indicating a chondrite-normalized value) and is calculable for one point. Due to the high light REE (LREE) and light element signal on the indium mounting medium, we were unable to calculate La concentrations for two of the three points and unable to calculate Ti concentrations for one point. Using the Ce/Ce* from spot 2b and using the average T^{xIIn} for the two points with usable Ti data (~660 ± 80 °C), we calculate redox conditions ~9 ± 1 log units below FMQ (after ref. 22). Data are shown in Table S4. Spot 2b, blue circles; spot 4, red triangles; spot 5, white stars. Spot 5 was collected after spot 4 in the same location.

Table S1. Measurements on the $^{12}C_2^+$ species on various materials, using either a 5-nA (zircon, inclusions, *E. coli*) or 2-pA (epoxy) Cs^+ primary beam

Sample	Material	$^{12}C_2^+$, cps	1 SD
ecoli.ais	Ecoli	3.89E+05	2.46E+04
ecoli@2.ais	Ecoli	4.19E+05	3.72E+04
ecoli@3.ais	Ecoli	5.83E+05	2.44E+04
ecoli@4.ais	Ecoli	5.16E+05	2.89E+04
Epoxy_MultiTest.ais	Epoxy	4.92E+04	2.48E+04
Epoxy_MultiTest@1.ais	Epoxy	2.39E+05	2.15E+04
Epoxy_MultiTest@10.ais	Epoxy	3.40E+05	2.35E+04
Epoxy_MultiTest@11.ais	Epoxy	3.42E+05	2.36E+04
Epoxy_MultiTest@12.ais	Epoxy	3.65E+05	2.47E+04
Epoxy_MultiTest@13.ais	Epoxy	3.86E+05	2.79E+04
Epoxy_MultiTest@14.ais	Epoxy	3.79E+05	2.46E+04
Epoxy_MultiTest@15.ais	Epoxy	3.81E+05	2.45E+04
Epoxy_MultiTest@16.ais	Epoxy	3.91E+05	2.50E+04
Epoxy_MultiTest@17.ais	Epoxy	3.96E+05	2.55E+04
Epoxy_MultiTest@18.ais	Epoxy	3.58E+05	2.07E+04
Epoxy_MultiTest@19.ais	Epoxy	4.31E+05	6.47E+04
Epoxy_MultiTest@2.ais	Epoxy	3.16E+05	2.20E+04
Epoxy_MultiTest@20.ais	Epoxy	3.96E+05	2.42E+04
Epoxy_MultiTest@21.ais	Epoxy	3.93E+05	2.51E+04
Epoxy_MultiTest@22.ais	Epoxy	3.87E+05	2.56E+04
Epoxy_MultiTest@3.ais	Epoxy	3.34E+05	2.30E+04
Epoxy_MultiTest@4.ais	Epoxy	3.27E+05	2.14E+04
Epoxy_MultiTest@5.ais	Epoxy	3.36E+05	1.91E+04
Epoxy_MultiTest@6.ais	Epoxy	3.43E+05	2.29E+04
Epoxy_MultiTest@7.ais	Epoxy	3.44E+05	2.20E+04
Epoxy_MultiTest@8.ais	Epoxy	3.29E+05	2.15E+04
Epoxy_MultiTest@9.ais	Epoxy	3.43E+05	2.51E+04
CC.ais	Epoxy	4.96E+05	1.17E+05
CC@1.ais	Epoxy	5.00E+05	1.43E+05
CC@2.ais	Epoxy	4.99E+05	1.42E+05
rses58_epoxy.ais	Epoxy	5.41E+05	1.28E+04
rses58_epoxy@1.ais	Epoxy	2.90E+05	6.71E+04
rses58_epoxy@2.ais	Epoxy	6.39E+05	9.04E+03
rses77epoxy@25.ais	Epoxy	6.50E+05	7.23E+03
rses77epoxy@26.ais	Epoxy	7.54E+05	3.99E+03
RSESepoxy.ais	Epoxy	3.87E+05	3.66E+03
RSESepoxy@1.ais	Epoxy	3.89E+05	3.59E+03
RSESepoxy@10.ais	Epoxy	4.24E+05	4.99E+03
RSESepoxy@11.ais	Epoxy	4.42E+05	2.93E+03
RSESepoxy@12.ais	Epoxy	4.39E+05	4.43E+03
RSESepoxy@13.ais	Epoxy	4.46E+05	3.26E+03
RSESepoxy@14.ais	Epoxy	4.33E+05	5.97E+03
RSESepoxy@15.ais	Epoxy	4.06E+05	2.26E+04
RSESepoxy@16.ais	Epoxy	4.25E+05	2.34E+04
RSESepoxy@17.ais	Epoxy	4.26E+05	2.32E+04
RSESepoxy@18.ais	Epoxy	4.33E+05	2.34E+04
RSESepoxy@19.ais	Epoxy	3.79E+05	3.05E+04
RSESepoxy@2.ais	Epoxy	3.97E+05	3.21E+03
RSESepoxy@20.ais	Epoxy	6.63E+05	6.86E+03
RSESepoxy@21.ais	Epoxy	6.70E+05	6.32E+03
RSESepoxy@22.ais	Epoxy	6.64E+05	6.26E+03
RSESepoxy@23.ais	Epoxy	6.58E+05	7.41E+03
RSESepoxy@24.ais	Epoxy	6.54E+05	7.71E+03
RSESepoxy@3.ais	Epoxy	3.78E+05	3.73E+03
RSESepoxy@4.ais	Epoxy	3.77E+05	5.16E+03
RSESepoxy@5.ais	Epoxy	3.84E+05	5.62E+03
RSESepoxy@6.ais	Epoxy	3.86E+05	5.38E+03
RSESepoxy@7.ais	Epoxy	3.86E+05	4.32E+03
RSESepoxy@8.ais	Epoxy	4.00E+05	5.13E+03
RSESepoxy@9.ais	Epoxy	4.09E+05	7.70E+03
rses58_7-9incl@1.ais	Surficial inclusion	1.69E+02	2.13E+01
rses58_7-9incl@2.ais	Surficial inclusion	1.85E+02	8.79E+01
rses58_7-9incl@3.ais	Surficial inclusion	2.03E+02	2.35E+01

Table S1. Cont.

Sample	Material	$^{12}C_2^+$, cps	1 SD
rses58_7-9incl@4.ais	Surficial inclusion	1.85E+02	1.60E+02
rses58_7-9incl@5.ais	Surficial inclusion	1.05E+02	7.15E+00
rses77_5-7crk@1.ais	Surficial inclusion	1.31E+02	2.35E+01
rses77_5-7crk@2.ais	Surficial inclusion	2.17E+04	3.93E+03
rses77_5-7qtz@1.ais	Surficial inclusion	1.90E+01	2.07E+00
rses77_5-7qtz@2.ais	Surficial inclusion	2.58E+02	6.18E+01
rses77_5-7qtz@3.ais	Surficial inclusion	1.27E+01	1.77E+00
rses77_5-7rut@1.ais	Surficial inclusion	1.90E+01	1.92E+00
MES1K_testR1@1.ais	Zircon, no presputter	2.22E+04	7.30E+03
SpLb_zirc2@1.ais	Zircon, no presputter	1.02E+05	1.11E+05
as3_test1.ais	Zircon, no presputter	1.61E+04	1.28E+04
as3_test1@1.ais	Zircon, no presputter	1.16E+04	2.10E+03
as3_test2.ais	Zircon, no presputter	1.96E+05	2.06E+05
as3_test2@1.ais	Zircon, no presputter	2.87E+04	8.57E+03
zircon.ais	Zircon, no presputter	7.00E+04	9.89E+03
zircon@1.ais	Zircon, no presputter	1.35E+04	4.95E+02
zircon@2.ais	Zircon, no presputter	2.93E+04	1.56E+03
zircon@3.ais	Zircon, no presputter	8.08E+03	1.66E+03
zircon@4.ais	Zircon, no presputter	2.90E+04	1.26E+03
zircon@5.ais	Zircon, no presputter	9.38E+03	5.41E+02
zircon@6.ais	Zircon, no presputter	5.11E+03	2.31E+03
zircon@7.ais	Zircon, no presputter	1.03E+04	1.79E+03
zircon@8.ais	Zircon, no presputter	2.29E+04	1.32E+03
MES1K_test2@1.ais	S-type granite zircon	7.31E+01	4.02E+01
MES1K_test2@2.ais	S-type granite zircon	3.43E+01	2.06E+01
MES1K_test3@1.ais	S-type granite zircon	1.08E+02	3.30E+01
MES1K_test3@2.ais	S-type granite zircon	1.83E+02	7.31E+01
MES1K_testR1.ais	S-type granite zircon	1.98E+00	3.28E+00
MES1K_testR1@2.ais	S-type granite zircon	6.32E+03	1.33E+03
MES1K_testR1@3.ais	S-type granite zircon	0.00E+00	0.00E+00
SpLb_zirc1@1.ais	A-type granite zircon	8.80E+00	2.25E+00
SpLb_zirc1@2.ais	A-type granite zircon	5.85E+00	1.76E+00
as3_test3.ais	Gabbro zircon	1.75E+03	3.54E+03
as3_test4.ais	Gabbro zircon	1.03E+02	3.98E+01
as3test4@1.ais	Gabbro zircon	4.34E+01	1.32E+01
as3test4@2.ais	Gabbro zircon	8.05E+02	9.01E+02
mes1k_test4@1.ais	S-type granite zircon	1.04E+03	2.08E+03
mes1k_test4@2.ais	S-type granite zircon	1.48E+03	2.50E+03
rg1a_zirc1@1.ais	Arc granite zircon	9.50E+00	3.93E+00
rg1a_zirc1@2.ais	Arc granite zircon	3.80E+00	1.60E+00
rg1a_zirc2@1.ais	Arc granite zircon	1.57E+01	5.88E+00
rg1a_zirc2@2.ais	Arc granite zircon	1.68E+02	2.59E+02
rg1a_zirc3@1.ais	Arc granite zircon	4.62E+01	3.24E+01
rg1a_zirc3@2.ais	Arc granite zircon	1.13E+01	4.95E+00
rses58_7-9blank@1.ais	Jack Hills zircon	1.40E+01	2.15E+00
rses77_3-7@1.ais	Jack Hills zircon	8.55E+01	5.76E+00
rses77_5-7blank.ais	Jack Hills zircon	1.86E+01	2.62E+00
rses77_6-6@1.ais	Jack Hills zircon	2.56E+01	3.23E+00
rses77_6-7@1.ais	Jack Hills zircon	3.32E+01	5.07E+00
zircon@9.ais	Jack Hills zircon	7.03E+01	4.88E+00

Table S2. Raw carbon isotopic measurements on mount RSES 61-18.8 (including epoxy, zircon background, indium background, and inclusion measurements) and *E. coli* secondary standard

Sample	Notes	$^{12}C_2^+$ signal, cps	1 SD	$^{12}C^{13}C^+$ signal, cps	1 SD
ecoli_test@1.ais	*E. coli* spot 1	3.41E+04	2.91E+03	7.48E+02	6.83E+01
ecoli_test@2.ais	*E. coli* spot 2	2.98E+04	4.63E+03	6.55E+02	1.00E+02
epoxy.ais	Epoxy	7.11E+05	4.03E+03	1.55E+04	1.20E+02
epoxy@1.ais	Epoxy	7.08E+05	1.24E+03	1.54E+04	7.03E+01
epoxy@2.ais	Epoxy	7.19E+05	1.06E+03	1.56E+04	8.15E+01
epoxy@3.ais	Epoxy	6.80E+05	2.20E+04	1.48E+04	4.73E+02
epoxy@4.ais	Epoxy	6.57E+05	6.54E+03	1.42E+04	1.69E+02
epoxy@5.ais	Epoxy	7.14E+05	1.14E+03	1.55E+04	7.46E+01
epoxy_final.ais	Epoxy	7.00E+05	7.80E+03	1.52E+04	1.80E+02
epoxy_final@1.ais	Epoxy	6.98E+05	7.56E+03	1.52E+04	1.53E+02
epoxy_last@1.ais	Epoxy	6.97E+05	8.05E+03	1.52E+04	1.80E+02
epoxy_new.ais	Epoxy	6.18E+05	2.43E+03	1.34E+04	7.95E+01
epoxy_test@1.ais	Epoxy	6.98E+05	3.08E+04	1.52E+04	6.58E+02
epoxy_test@10.ais	Epoxy	6.89E+05	2.88E+04	1.50E+04	6.43E+02
epoxy_test@2.ais	Epoxy	7.32E+05	1.00E+04	1.59E+04	2.30E+02
epoxy_test@3.ais	Epoxy	7.45E+05	6.87E+03	1.62E+04	1.86E+02
epoxy_test@4.ais	Epoxy	7.54E+05	6.11E+03	1.64E+04	1.30E+02
epoxy_test@5.ais	Epoxy	7.58E+05	1.29E+04	1.65E+04	3.06E+02
epoxy_test@6.ais	Epoxy	7.77E+05	9.34E+03	1.69E+04	2.08E+02
epoxy_test@7.ais	Epoxy	7.90E+05	7.12E+03	1.72E+04	1.69E+02
epoxy_test@8.ais	Epoxy	8.02E+05	8.56E+03	1.75E+04	1.97E+02
epoxy_test@9.ais	Epoxy	7.05E+05	2.49E+04	1.53E+04	5.51E+02
indium.ais	Indium (background)	5.08E+01	7.90E+00	1.21E+00	4.16E-01
indium@1.ais	Indium (background)	2.19E+03	4.47E+02	4.68E+01	9.66E+00
indium@2.ais	Indium (background)	2.24E+03	2.37E+02	4.86E+01	6.30E+00
indium@3.ais	Indium (background)	1.46E+03	4.70E+02	3.18E+01	9.88E+00
indium@4.ais	Indium (background)	1.77E+03	6.77E+02	3.89E+01	1.39E+01
indium@5.ais	Indium (background)	1.95E+03	7.04E+02	4.28E+01	1.77E+01
indium@6.ais	Indium (background)	2.75E+03	1.27E+03	5.75E+01	2.69E+01
indium@7.ais	Indium (background)	2.45E+03	5.06E+02	5.27E+01	1.10E+01
indium@8.ais	Indium (background)	5.60E+03	2.61E+03	1.25E+02	5.95E+01
zircon@1.ais	Zircon spot 1	7.07E+01	7.72E+00	1.86E+00	1.03E+00
zircon@2.ais	Zircon spot 1	9.06E+01	8.70E+00	2.09E+00	7.22E-01
zircon@3.ais	Zircon spot 1	6.85E+03	5.51E+03	1.49E+02	1.16E+02
zircon@4.ais	Zircon spot 1	3.70E+03	8.38E+02	8.09E+01	1.94E+01
zircon@5.ais	Zircon spot 1	7.03E+03	2.63E+03	1.52E+02	5.66E+01
zircon@6.ais	Zircon spot 1	1.66E+04	9.41E+03	3.58E+02	2.10E+02
zircon@7.ais	Zircon spot 1	4.60E+03	1.16E+03	9.85E+01	2.38E+01
zircon@8.ais	Zircon spot 1	4.00E+03	1.10E+03	8.59E+01	2.52E+01
zircon@9.ais	Zircon spot 1	2.59E+03	8.07E+02	5.59E+01	1.69E+01
zircon@10.ais	Zircon spot 1	1.97E+03	7.28E+02	4.20E+01	1.39E+01
zircon@11.ais	Zircon spot 1	1.54E+03	7.34E+02	3.24E+01	1.43E+01
zircnewspot@1.ais	Zircon spot 2	2.17E+04	8.09E+03	4.68E+02	1.77E+02
zircnewspot@2.ais	Zircon spot 2	1.25E+01	1.85E+00	3.75E-01	3.67E-01
zircon_try3.ais	Zircon spot 3	6.03E+03	2.05E+03	1.29E+02	4.80E+01
zircon_try3@1.ais	Zircon spot 3	9.51E+03	3.64E+03	2.04E+02	7.88E+01
zircon_try3@2.ais	Zircon spot 3	2.58E+04	1.18E+04	5.61E+02	2.56E+02
zircon_try3@3.ais	Zircon spot 3	9.28E+04	5.68E+04	2.03E+03	1.25E+03
zircon_try3@4.ais	Zircon spot 3	1.11E+05	4.28E+04	2.42E+03	9.33E+02
zircon_try3@5.ais	Zircon spot 3	4.00E+04	2.99E+04	8.66E+02	6.31E+02
zircon_try3@6.ais	Zircon spot 3	2.59E+04	2.42E+04	5.63E+02	5.25E+02
zircon_try3@7.ais	Zircon spot 3	1.75E+04	5.36E+03	3.80E+02	1.17E+02
zircon_try4@1.ais	Zircon spot 4	4.16E+03	5.40E+02	9.08E+01	1.25E+01
zircon_try4@2.ais	Zircon spot 4	4.76E+03	1.08E+03	1.04E+02	2.34E+01
zircon_try4@3.ais	Zircon spot 4	6.04E+03	1.61E+03	1.34E+02	3.43E+01
zircon_try4@4.ais	Zircon spot 4	5.53E+03	1.51E+03	1.20E+02	3.40E+01
zircon_try4@5.ais	Zircon spot 4	3.55E+03	1.13E+03	7.82E+01	2.47E+01
zircon_try4@6.ais	Zircon spot 4	2.42E+03	1.11E+03	5.34E+01	2.47E+01
zircon_try5@1.ais	Zircon spot 5	5.22E+03	2.49E+03	1.13E+02	5.35E+01
zircon_try5@2.ais	Zircon spot 5	3.02E+03	8.77E+02	6.67E+01	2.09E+01
zircon_try5@3.ais	Zircon spot 5	1.85E+03	2.24E+02	4.00E+01	6.12E+00
zircon_try6.ais	Zircon spot 6	3.39E+02	2.24E+02	7.45E+00	4.38E+00

Table S2. Cont.

Sample	Notes	$^{12}C_2^+$ signal, cps	1 SD	$^{12}C^{13}C^+$ signal, cps	1 SD
zircon_try6@1.ais	Zircon spot 6	1.58E+02	3.03E+01	3.03E+00	1.06E+00
zircon_try6@2.ais	Zircon spot 6	1.28E+02	1.46E+01	2.80E+00	1.13E+00
zircon_try7.ais	Zircon spot 7	9.12E+03	4.22E+03	1.95E+02	8.92E+01
zircon_try8.ais	Zircon spot 8	1.02E+05	5.05E+04	2.22E+03	1.09E+03
zircon_try8@1.ais	Zircon spot 8	8.50E+04	2.82E+04	1.84E+03	6.07E+02
zircon_try8@2.ais	Zircon spot 8	5.58E+04	1.35E+04	1.21E+03	2.86E+02
zircon_try8@3.ais	Zircon spot 8	4.98E+04	3.92E+03	1.09E+03	8.44E+01
zircon_try8@4.ais	Zircon spot 8	5.52E+04	3.33E+03	1.20E+03	8.14E+01
zircon_try8@5.ais	Zircon spot 8	6.00E+04	4.24E+03	1.31E+03	8.40E+01

Each analysis represents 20 cycles counting on $^{12}C_2^+$ and $^{12}C^{13}C^+$ and were undertaken in multicollection mode. Measurements on epoxy used a 2-pA Cs^+ primary beam and those on the other materials a 5-nA beam.

Table S3. Corrected $\delta^{13}C$ for isotopic measurements in Table S2

Sample	$\delta^{13}C$, uncorrected	1 SD	Corrected $\delta^{13}C$	1 SD	Use $\delta^{13}C$?
ecoli_test@1.ais	−24.75	4.32	−20.18	3.63	Yes
ecoli_test@2.ais	−21.24	5.88	−17.32	4.85	Yes
epoxy.ais	−32.02	1.14	−26.11	1.44	Yes
epoxy@1.ais	−32.53	0.72	−26.53	1.27	Yes
epoxy@2.ais	−32.90	1.15	−26.83	1.47	Yes
epoxy@3.ais	−32.02	0.82	−26.11	1.29	Yes
epoxy@4.ais	−35.38	1.18	−28.85	1.56	Yes
epoxy@5.ais	−33.66	0.97	−27.45	1.40	Yes
epoxy_final.ais	−31.27	0.86	−25.50	1.29	Yes
epoxy_final@1.ais	−29.30	0.84	−23.90	1.22	Yes
epoxy_last@1.ais	−30.44	0.80	−24.82	1.24	Yes
epoxy_new.ais	−31.66	1.08	−25.82	1.41	Yes
epoxy_test@1.ais	−30.88	1.02	−25.18	1.35	Yes
epoxy_test@10.ais	−32.86	0.75	−26.80	1.29	Yes
epoxy_test@2.ais	−30.97	1.05	−25.26	1.37	Yes
epoxy_test@3.ais	−32.74	1.02	−26.70	1.40	Yes
epoxy_test@4.ais	−30.37	0.92	−24.76	1.29	Yes
epoxy_test@5.ais	−31.68	0.96	−25.83	1.34	Yes
epoxy_test@6.ais	−32.77	0.75	−26.72	1.28	Yes
epoxy_test@7.ais	−31.77	0.62	−25.91	1.21	Yes
epoxy_test@8.ais	−30.50	0.66	−24.87	1.18	Yes
epoxy_test@9.ais	−31.94	0.99	−26.05	1.37	Yes
indium.ais	76.89	86.00	62.70	70.19	
indium@1.ais	−47.33	16.87	−38.59	13.85	
indium@2.ais	−36.39	13.35	−29.68	10.96	
indium@3.ais	−29.03	19.09	−23.68	15.60	
indium@4.ais	−12.54	20.94	−10.23	17.09	
indium@5.ais	−29.37	19.39	−23.95	15.84	
indium@6.ais	−66.50	16.10	−54.23	13.33	
indium@7.ais	−42.40	13.04	−34.57	10.73	
indium@8.ais	−15.05	10.23	−12.27	8.36	
zircon@1.ais	172.79	153.32	140.91	125.17	
zircon@2.ais	39.98	89.20	32.60	72.76	
zircon@3.ais	−23.71	12.52	−19.34	10.24	
zircon@4.ais	−29.12	11.09	−23.75	9.10	
zircon@5.ais	−33.95	9.11	−27.69	7.52	
zircon@6.ais	−47.43	8.47	−38.68	7.10	
zircon@7.ais	−43.76	10.11	−35.68	8.38	
zircon@8.ais	−45.65	9.19	−37.23	7.66	
zircon@9.ais	−38.68	12.86	−31.54	10.57	
zircon@10.ais	−38.50	17.57	−31.40	14.39	
zircon@11.ais	−50.58	18.56	−41.24	15.23	
zircnewspot@1.ais	−40.15	4.06	−32.74	3.59	
zircnewspot@2.ais	368.92	321.32	300.85	262.34	
zircon_try3.ais	−55.84	10.64	−45.54	8.89	
zircon_try3@1.ais	−43.43	9.01	−35.42	7.50	
zircon_try3@2.ais	−32.84	5.79	−26.78	4.85	Yes
zircon_try3@3.ais	−31.36	3.28	−25.58	2.89	Yes
zircon_try3@4.ais	−29.98	2.86	−24.44	2.55	Yes
zircon_try3@5.ais	−25.39	6.12	−20.70	5.07	Yes
zircon_try3@6.ais	−29.15	5.20	−23.77	4.36	Yes
zircon_try3@7.ais	−29.09	6.33	−23.73	5.26	Yes
zircon_try4@1.ais	−29.19	10.00	−23.80	8.21	
zircon_try4@2.ais	−29.96	13.08	−24.43	10.72	
zircon_try4@3.ais	−11.44	9.89	−9.33	8.08	
zircon_try4@4.ais	−38.37	13.10	−31.29	10.76	
zircon_try4@5.ais	−16.24	15.65	−13.25	12.78	
zircon_try4@6.ais	−17.29	16.58	−14.10	13.53	
zircon_try5@1.ais	−36.24	10.40	−29.55	8.57	
zircon_try5@2.ais	−21.21	12.01	−17.30	9.82	
zircon_try5@3.ais	−35.46	18.93	−28.92	15.49	
zircon_try6.ais	14.64	39.61	11.94	32.31	
zircon_try6@1.ais	−158.01	53.69	−128.86	44.12	

Table S3. Cont.

Sample	$\delta^{13}C$, uncorrected	1 SD	Corrected $\delta^{13}C$	1 SD	Use $\delta^{13}C$?
zircon_try6@2.ais	−34.08	79.48	−27.79	64.82	
zircon_try7.ais	−45.96	7.80	−37.48	6.56	
zircon_try8.ais	−29.52	2.33	−24.07	2.16	Yes
zircon_try8@1.ais	−33.64	3.55	−27.44	3.12	Yes
zircon_try8@2.ais	−32.26	4.40	−26.31	3.76	Yes
zircon_try8@3.ais	−29.12	3.31	−23.75	2.88	Yes
zircon_try8@4.ais	−29.02	4.07	−23.67	3.47	Yes
zircon_try8@5.ais	−26.70	2.89	−21.77	2.53	Yes

Each analysis represents 20 cycles counting on $^{12}C_2^+$ and $^{12}C^{13}C^+$ and were undertaken in multicollection mode. Measurements on epoxy used a 2-pA Cs^+ primary beam and those on the other materials a 5-nA beam.

Table S4. Trace element data for RSES 61-18.8

Sample	rses61-18.8 spot 2b	1σ	rses61-18.8 spot 4	1σ	rses61-18.8 spot 5	1σ	Average	1σ
Mg	—	—	—	—	—	—	—	—
Mn	—	—	—	—	—	—	—	—
P	176.29	51.05	56.08	13.57	—	—	116.19	85.00
Ti	5.69	1.84	1.49	0.43	—	—	3.59	2.97
Fe	179.78	41.53	141.01	32.90	123.55	28.65	148.11	28.78
Y	1,341.22	1,415.27	1,448.42	1,529.98	1,451.76	1,531.81	1,413.80	62.88
La	0.56	0.22	—	—	—	—	0.56	0.22
Ce	14.10	4.52	8.38	2.50	5.33	1.59	9.27	4.45
Pr	1.00	0.46	0.24	0.10	0.21	0.08	0.49	0.45
Nd	29.09	9.53	9.69	3.06	8.22	2.59	15.67	11.65
Sm	14.38	6.47	7.50	3.26	7.68	3.33	9.85	3.92
Eu	2.11	0.92	1.77	0.77	1.83	0.80	1.90	0.18
Gd	27.54	12.02	26.28	11.01	26.34	11.01	26.72	0.71
Tb	10.77	4.76	11.74	5.05	11.32	4.85	11.28	0.48
Dy	119.49	46.89	125.73	49.48	126.49	49.69	123.90	3.84
Ho	44.00	24.12	46.97	25.24	47.98	25.64	46.32	2.07
Er	173.69	93.79	191.05	103.92	191.01	103.31	185.25	10.01
Tm	35.48	19.56	39.49	21.79	39.93	22.12	38.30	2.45
Yb	317.35	210.71	356.43	233.70	358.81	234.33	344.20	23.28
Lu	64.12	36.34	71.15	39.85	72.40	40.33	69.22	4.46
Hf	7,764.16	2,504.26	7,603.65	2,470.71	7,952.39	2,566.42	7,773.40	174.55
Th	138.10	65.05	63.20	26.89	56.10	23.34	85.80	45.43
U	116.59	46.54	98.02	37.39	105.82	40.19	106.81	9.33
La (N)	2.36		—	—	—	—	2.36	
Ce (N)	23.00		13.67		8.70		15.12	
Pr (N)	10.79		2.62		2.30		5.24	
Ce/Ce*	4.56	23.55					4.30	43.45
Txlln	694	27	597	19	—	—	658	81
ΔFMQ	−8	1					−9	2
ΔFMQ†	−9	1						

Concentrations are in ppm; temperatures (T^{xlln}) are in degrees Celsius; "ΔFMQ" represents $\log_{10}$ units of oxygen fugacity f_{O2} relative to the fayalite–magnetite–quartz buffer. All data presented are corrected for the trace element background measured on the indium mounting medium. Corrected abundances were then standardized to National Institute of Standards and Technology 610 zircon, with additional correction of the ^{49}Ti abundance based on the 91500 zircon standard (37, 38). Using the calculated $Ce/Ce^* = [Ce]/([La] \times [Pr])^{1/2}$ and T^{xlln} from point 2b, reduced conditions characterized by ΔFMQ = −8 ± 1 are inferred. [La] was not available for the other spots. Using the T^{xlln} calculated from average [Ti], this spot yields a ΔFMQ = −9 ± 1. Using average abundances from all spots yields ΔFMQ = −9 ± 2. T^{xlln} was calculated from ref. 9; f_{O2} was calculated from ref. 22.

†This calculation uses the T^{xlln} from average [Ti] and spot 2b's Ce/Ce*.

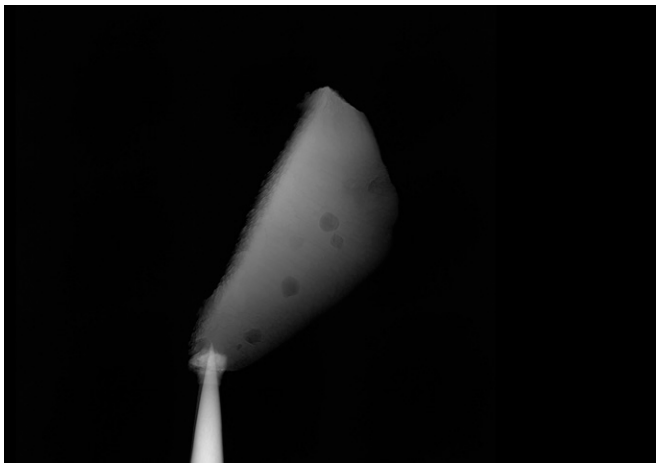

Movie S1. FIBed section of RSES 61-18.8, imaged by transmission X-ray microscopy. The section is rotated around a tungsten needle attached to one end. Several fully enclosed inclusions are visible. Fig. 1 of the main text points out the carbonaceous phases. Imaging is by Crystal Shi (Department of Earth, Energy, and Environmental Sciences, Stanford University, Stanford, CA).

Movie S1

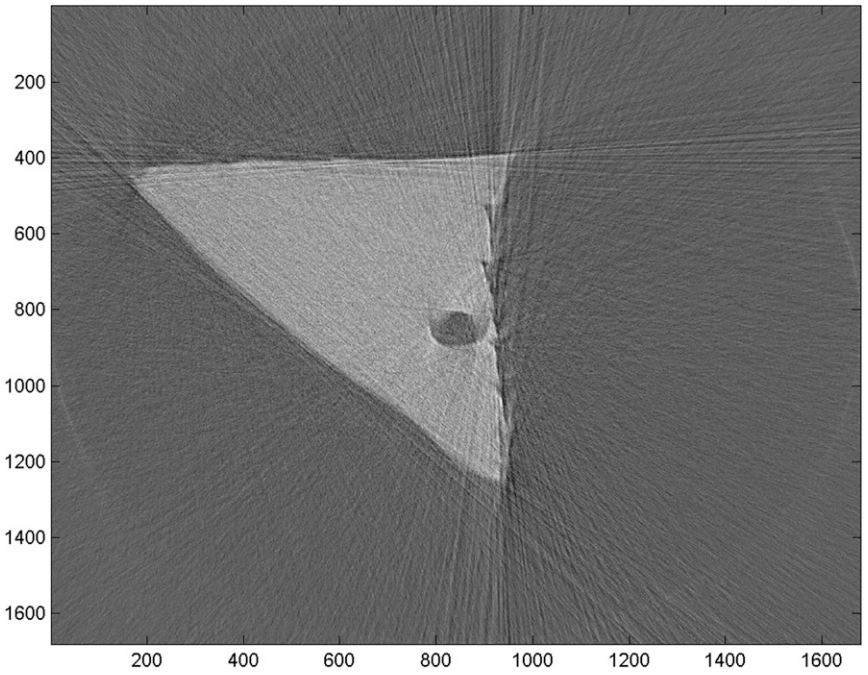

Movie S2. Reconstruction of the image slices from the X-ray microscopy, showing slices roughly perpendicular to the tungsten needle and beginning at the tip of the zircon section opposite the needle. Several fully enclosed inclusions are visible. Fig. 1 of the main text points out the carbonaceous phases. Reconstructions are by Elizabeth Boehnke (Radiation Oncology Department, Cedars Sinai Medical Center, Los Angeles).

Movie S2